Developing a predictive model for the chemical composition of soot nanoparticles

Lead PI: A. Violi

University of Michigan

Ann Arbor, MI

Collaborators:

N. Hansen, H. Michelsen

Combustion Research Facility - Sandia National Laboratories

Background and Significance

Transportation sector, which dominates demand for liquid fuels, is responsible for the second largest portion of energy use in the U.S., trailing industrial consumption by only a few percent. According to this report, the total U.S. consumption of liquid fuels, including both petroleum-based fuels and biofuels, is expected to increase from 37.0 quadrillion Btu (18.9 million barrels per day) in 2011 to 37.6 quadrillion BTU (19.8 million barrels per day) in 2019, then reaching 36.1 quadrillion Btu in 2040. Transportation fuels are currently produced mainly by refining petroleum-based sweet crude oil, from which gasoline, diesel fuel, and jet fuel are each made with specific physical and chemical characteristics dictated by the type of engine in which they are to be burned. New fuels with different characteristics are emerging to displace crude oil, and new engine technologies are under development, promising improved efficiency and emissions.

Indeed, mobile sources are responsible for direct emissions of air toxics and contribute to precursor emissions, which react to form secondary pollutants. Recently the Environmental Protection Agency announced a new air pollution standard that will bring 20% reduction in microscopic particles of soot emitted by coal-fired power plants and diesel vehicles by 2020. The EPA estimated that by 2030, the reduction in soot "from diesel vehicles and equipment alone" could prevent up to 40,000 premature deaths and 4.7 million days of work lost due to illness. Growing evidence suggests that the environmental and human health effects of soot are directly related to the particle size distribution and chemical composition. These characteristics will need to be taken into consideration for future regulatory developments.

Development of advanced combustion modeling capabilities is crucial for providing a scientific foundation behind technology breakthroughs in transportation fuels, such as those involving optimizing the operation and design of evolving fuels as well as reducing emissions. Current models for soot formation are overly simplistic, and the mechanisms of particle nucleation and mass growth remain semi-empirical and phenomenological. Since the kinetics of nucleation control the number of nascent particles, and the coagulation of these particles

determine the evolution of particle number density, current models are not able to predict particle formation and evolution in various combustion conditions.

Next generation soot models should have the ability to predict the particle size distribution functions and describe and follow the kinetic evolution of surface and interior chemical composition. Both features are critical to achieving the next level of understanding of the various processes of soot formation, including nucleation, mass growth. In this project we have investigated the formation of particles in combustion environments and developed a novel and detailed theoretical model that describes nanoparticle inception and provide information on their chemical structure and composition. The phenomenon of particle inception influences the chemical compositions of nanoparticles. The model has been guided and validated by experimental data produced by the research groups of Michelsen and Hansen at Sandia National Laboratories and Wilson at Lawrence Berkeley National Laboratory.

This work provides novel insight into the chemical composition of nanoparticles in flames, which substantially influences physical agglomeration phenomena. An experimentally validated, predictive model for the chemical composition of soot nanoparticles will enhance our understanding of soot formation and will allow the prediction of particle size distributions in combustion conditions. Recent studies show that the chemical and physical properties of nanoparticles affect the coagulation behavior to form soot. This predictive capability, if attained, will fundamentally change the modeling of soot formation by establishing a scientific understanding of sufficient depth and flexibility to facilitate realistic simulation of fuel combustion and particle formation in more complex systems, such as existing and proposed engines.

Objectives

The goal of this proposal has been to study the formation mechanisms of nanoparticles in order to develop a model that could be predictive code for the chemical composition of nanoparticles produced in laminar flames. To this end, we combined stare-of-the-art computational and experimental techniques to study the formation of combustion-generated products as a combination of chemical and physical reactions of gas-phase species. Several experimental tools, described in more detail below, have been used to refine the identification of molecular species associated with the formation of various species in flames. Experimental evidence for specific functional groups will be used to identify and constrain nucleation mechanisms in the model and provide information on the chemical compositions of nanoparticles.

In the following sections, we report a description of the approaches and the synergistic results achieved over the last period. The work has been conducted by Prof. Angela Violi at the University of Michigan (modeling), Dr. Hope Michelsen at Sandia National Laboratories. Kevin Wilson is an unfunded collaborator at Lawrence Berkeley National Laboratory (LBNL). The experiments described here are strongly tied to the computational work led by Angela Violi. The foundation of this work is the development of a tight relationship between the experimental and computational components of the project. Our team works closely and concertedly to integrate the measurements with the theory and simulations. We design our experiments to facilitate the simulations, and use the simulations to drive the experiments.

Approaches and Results

Soot formation involves growth of hydrocarbon species to produce gas-phase precursors and nucleation of these precursors to generate condensed-phase particles, but there are large gaps in our understanding of the fundamental chemical physics of steps involved in this process. There is considerable evidence to suggest that soot formation is tightly linked to production of polycyclic aromatic hydrocarbon (PAH) species, and it is generally assumed that large PAHs are the critical precursor to particle inception.[1] However, the description of the formation pathways for these gas-phase particle precursors is fraught with uncertainties. More work is needed to establish the chemical mechanisms for the growth of these species.

In addition to uncertainties about gas-phase precursor formation, incipient particle nucleation is even more poorly understood and is perhaps the least well understood step in soot formation.[2] Although large PAHs appear to be linked to soot formation, it is not known what species characteristics or which species trigger particle inception and how this nucleation process occurs. Recent theoretical studies have suggested that PAHs with fewer than ~10 aromatic rings are unable to nucleate under typical atmospheric flame conditions.[3] Particle nucleation may involve factors other than molecular size, however, such as ionic charge,[4] aliphatic side chains on PAHs,[3a, 5] aliphatic bridges between PAHs,[5b, 6] aromatic-radical character,[3b] and oxygenated functional groups.[5b, 7]

This work focuses on identifying the species and mechanisms involved in soot formation. Once the atomic composition and structure of the soot-precursor molecules have been established, molecular sizes and physio-chemical pathways that lead to nucleation can be established. The presented work has a special emphasis on investigating the roles of radical-radical reactions and large oxygenated species in incipient particle formation. Many of the species recorded in mass spectra of incipient particles are not large (i.e., ≤400 u),[6a, 8] but larger species may be difficult to detect in most aerosol mass spectrometers. Some of these species may be condensed onto the particles from the gas phase during extraction from the flame. Many of the species observed in particles, at least under some conditions, appear to be oxygenated.[5b, 9] Our recent work has shown that predictions of large oxygenated species are consistent with these observations when the appropriate reactions are included in simulations.[9]

The work at Sandia is led by Hope Michelsen and ties strongly to the soot diagnostics program Our work over the past funding cycle targeted the molecular growth chemistry of soot-precursor molecules by combining aerosol mass spectrometry (AMS) using vacuum ultraviolet (VUV) light from the Advanced Light Source (ALS) at LBNL for chemical composition, X-ray photoelectron spectroscopy (XPS) for determination of functional groups, and atomistic stochastic modeling for studies of different chemical pathways.

***Particle composition*:** Our work to date has been largely based on applications of aerosol mass spectrometry using vacuum-ultraviolet photoionization (VUV-AMS) to study incipient-particle and precursor composition. An illustration of the ALS aerosol mass spectrometer is shown in Fig. 1. Particles are extracted from the flame through a quartz probe, are focused into a particle beam in an aerodynamic-lens system (ADL), and impinge on a heated target where they are vaporized. The gas-phase species are ionized with VUV synchrotron radiation that is tunable between 7.4 and 11.2 eV. This ionization approach allows for single-photon ionization of large

organic species, which reduces the probability of fragmentation of these species, a common complication with electron-ionization sources. The tunable photon source also permits investigations of the ionization efficiency as a function of photon energy, which can provide some structural information.

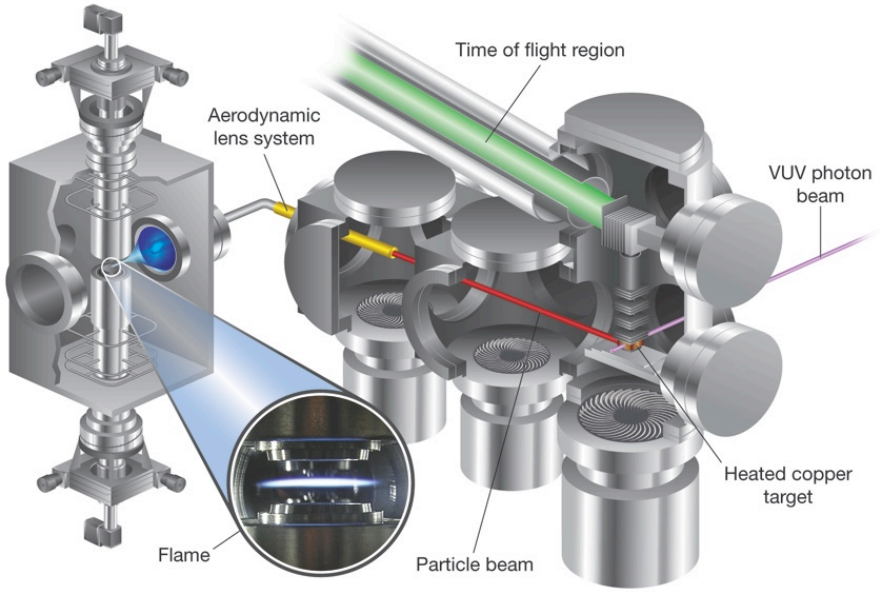

Figure 1. Schematic diagram of the ALS aerosol mass spectrometer attached to a counter-flow diffusion burner assembly.

All of these measurements have been made at selected locations in ethylene flames running at atmospheric pressure. For this project, we have used two flame configurations of interest (shown in Fig. 2). The first is the laminar premixed flat flame in which the chemistry and fluid dynamics can be decoupled, species concentrations and temperature change only as a function of the distance from the burner, and the role of oxygen in soot chemistry can be tested by changing the equivalence ratio. In the counter-flow diffusion flame, the species concentrations and temperature distributions are also quasi-one-dimensional and change as a function of the location between the burners, but the flow characteristics play an important role in the formation, growth, and oxidation of soot, and the simulations are more challenging.

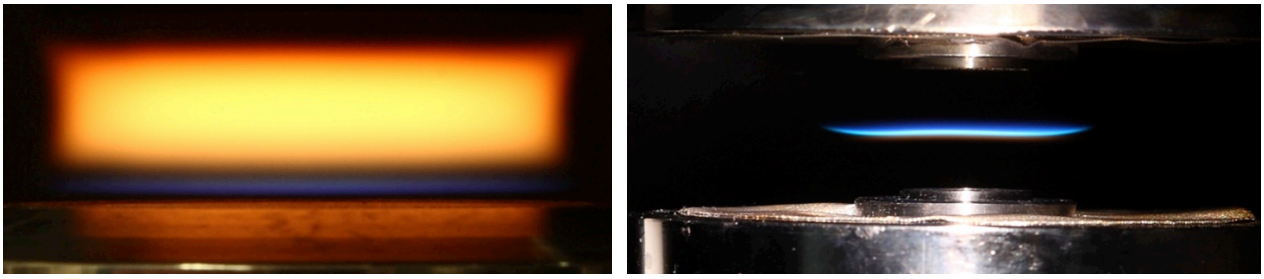

Figure 2. Target flames. (left) Laminar premixed flat flame, (right) Counter-flow diffusion flame.

***Large oxygenated hydrocarbon formation*:**[9] Furans are in a class of oxygenated hydrocarbons that are commonly emitted in exhaust plumes of combustion sources. Oxygenated hydrocarbons produced during combustion can have a wide range of detrimental effects on human health, air quality, and regional and global climate. Furans are compounds that contain five-membered rings with four carbon atoms and one oxygen atom. Many studies have shown that they are toxic and carcinogenic, whether ingested or inhaled, and thus pose a considerable threat to human health.[10] The simplest of these compounds (*i.e.*, unsubstituted furan, C_4H_4O) is a cyclic, dienyl ether with a low molecular weight, high volatility, and high lipophilicity. Despite the impact of large oxygenated hydrocarbons on combustion chemistry, the environment, and human health, very little is known about their formation mechanisms and emissions. Our work has demonstrated the formation of large oxygenated compounds, including furans, during the combustion of very simple hydrocarbon fuels.[9] Via a synergistic approach that includes *ab initio* methods and a stochastic model in conjunction with experimental measurements, we identified reaction pathways leading to formation of oxygenated compounds during the combustion of ethylene.

We recorded VUV-AMS spectra of particles sampled from premixed and diffusion flames. Figure 3 shows VUV-AMS spectra measured from particles extracted from a premixed flat flame at three different heights-above-burner (HABs). Based on mass, peaks shown in red were identified as entirely or partly stemming from species containing oxygen atoms at certain HABs. The spatial distributions of the oxygenated species are very different from those of pure hydrocarbon species and are weighted very heavily toward the oxygen side of the flame front relative to pure hydrocarbon species. Thus, peaks stemming entirely from oxygenated species, e.g., the peak at 160 u go away at high HABs in the premixed flame (Fig. 3), where there is no reactive oxygen available. Peaks that contain contributions from both oxygenated and non-oxygenated species, e.g., 194 u and 220 u tend to decrease in intensity and slightly shift their mass locations when moving away from the flame zone containing reactive oxygen, i.e., increasing HAB in the premixed flame (Fig. 3). A shift in mass location of a mass peak is consistent with a change in atomic constituents contributing to the signal. Hence, the mass shifts measured with increasing HAB for many of the peaks marked in red in Fig. 3 are attributable to a change in constituents contributing to a mass peak from predominantly oxygenated species to predominantly pure hydrocarbon species. The masses of the oxygenated species agree well with the atomic compositions predicted by the simulations. Both experiments and simulations demonstrate that ~50% of the mass peaks observed at some flame heights in the mass range 140 – 350 u contain signal from oxygenated species.

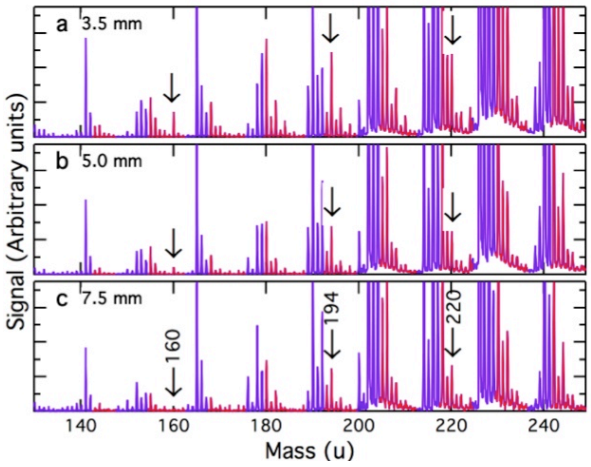

Figure 3. AMS spectra from a premixed flame. Mass spectra are shown for particles extracted from HABs of (**a**) 3.5, (**b**) 5.0, and (**c**) 7.5 mm. Red peaks contain signal from oxygenated species.

The predicted structures for these species are predominantly alcohols or enols near the burner or fuel outlet (for the counter-flow flame) and are mainly furans or ethers far from the burner or fuel outlet (e.g., Fig. 4).

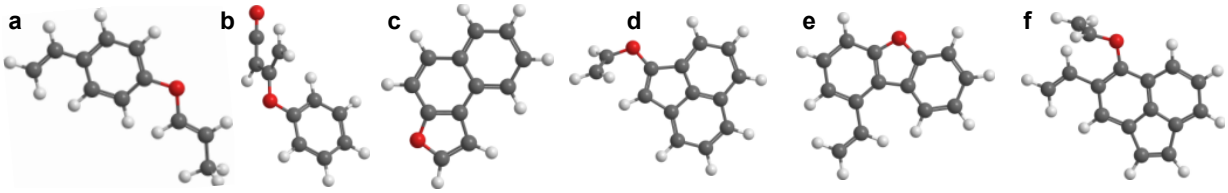

Figure 4. Frequently predicted oxygen-containing structures of selected masses low in a premixed flame. Red atoms: oxygen, gray: carbon, white: hydrogen. **a**-**b**, 160 u – ether, ether/ketene. **c**, 168 u – furan. **d**-**e**, 194 u – ether, furan. **f**, 220 u – ether.

The mass spectra yield masses and some elemental information, but they do not provide functional group information. In order to identify functional groups, we measured XPS spectra at the oxygen *K* edge, as shown in Fig. 5. These results support the prediction of alcohols and enols lower in the flame and a preference for ethers and furans at larger HABs.

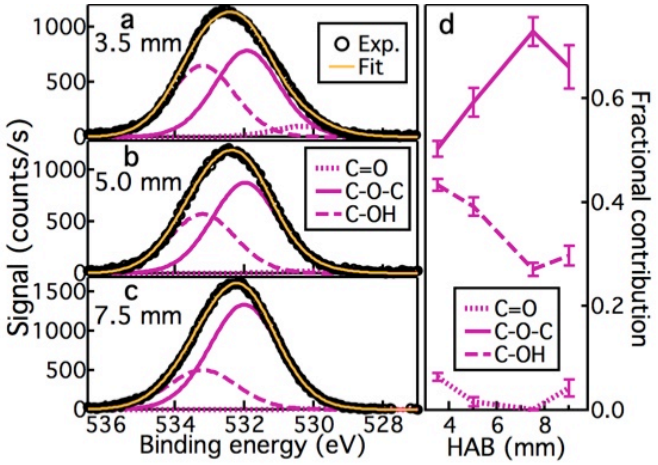

Figure 4.1.5. XPS O 1s spectra of soot sampled from a premixed flame. Spectra are shown for particles extracted from HABs of (**a**) 3.5 mm, (**b**) 5.0 mm, and (**c**) 7.5 mm. (**d**) Fractional

contributions of oxygenated functional groups were inferred from fits to XPS O 1s spectra. Error bars are ± one standard deviation of the uncertainties associated with the peak fits.

The most probable pathway to furan formation is shown in Figure 6 and starts with H-abstraction from a PAH edge site followed by addition of OH or O_2. The most probable pathway for embedding oxygen into the hydrocarbon molecules is *via* ethers formed when H is abstracted from hydroxyl groups or OH/O is abstracted from peroxy acid/radical groups, followed by hydrocarbon addition to the oxyradical and furan-ring closure. Acetylene is the most frequently added hydrocarbon. We expect this scheme to be important to a wide range of hydrocarbon oxidation processes and hydrocarbon-combustion systems because of high acetylene concentrations and low reaction barriers.

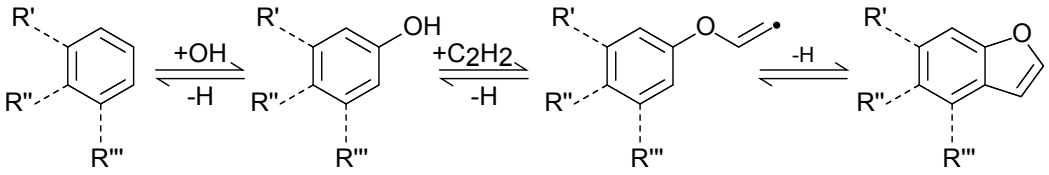

Figure 6. Most probable reaction sequence leading to formation of a furan group. Left-to-Right: H-abstraction followed by OH addition to the radical free-edge site on an aromatic ring; H-abstraction from the OH group, followed by acetylene addition, forming an ether group; H-elimination during ring closure to form a furan group.

***Radical-radical reactions*:**[8b] Nucleation of PAHs is thought to play a central role in particle inception, but the critical characteristics of these species are unknown. Some theoretical studies have indicated that molecular size is the limiting factor in homogeneous nucleation under flame conditions.[3, 5a] Mass spectrometric measurements of hydrocarbons formed in sooting flames suggest that the majority of these species are relatively small compared with the minimum size of ~10 aromatic rings for PAHs predicted to be involved in particle inception.[3, 5a] We have studied the formation of larger PAHs via radical-radical reactions involving large radical species.[8b] Figure 7 shows VUV-AMS spectra recorded on samples extracted from a premixed flat flame and a counter-flow diffusion flame. Peaks that stand out in these mass spectra include 226 u, 250 or 252 u, 266 u, 278 u, and 350 u, which is consistent with previous observations.[8b, 8c, 11] Siegmann *et al*.[11a] reported that species at 252 u and 350 u formed more rapidly earlier in the flame than other species of similar molecular weight in laminar methane diffusion flames. They proposed a reactive dimerization mechanism in which stable PAH molecules, such as naphthalene and anthracene, dimerized. The species at 350 u appears to grow more rapidly than several lighter ones, including the species at 202 u and 226 u in the counter-flow flame under study. The signal at 252 u shows a similar but weaker trend. We have previously shown that the

species at 266 u and 278 u grow ahead of lighter structures in an acetylene counter-flow diffusion flame,[8c] and the same trend is observed in the two flames under study.

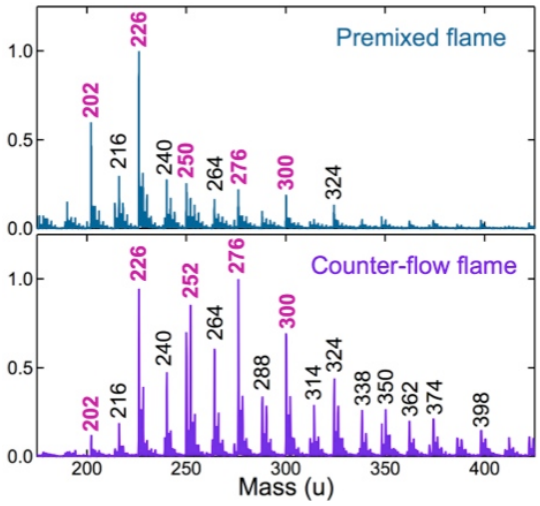

Figure 7. Aerosol mass spectra recorded at (top) HAB = 3.4 mm in the premixed flame and (bottom) distance from the fuel outlet (DFFO) = 3.0 mm in the counter-flow flame.

This effect is demonstrated in Fig. 8, which shows burner profiles, i.e., the normalized signal for selected masses in extracted particles as a function of HAB. The burner profiles for 266 u and 278 u are weighted toward lower HABs than those for 226 u and 202 u.

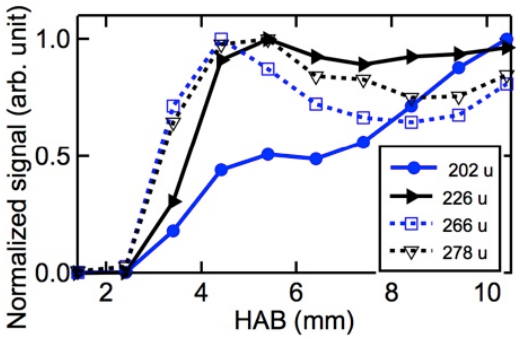

Figure 8. Normalized signal intensities for the mass peaks at 202 u, 226 u, 266 u, and 278 u as functions of HAB in the premixed flame

The Stochastic NAnoParticle Simulator (SNAPS)[12] predicts that, at an HAB of 3.4 mm, the probability of forming species with 202 u and 226 u is higher than that of forming 266 u and 278 u. A large number of radicals containing 1-20 carbon atoms is also predicted, and, if combined, they change the relative amounts of species at the masses shown in Fig. 8. We estimated the importance of combination pathways of these radicals by considering the frequency of collision of the various radicals and assuming a collision efficiency of 0.85. Negligible amounts of masses 202 and 226 u are formed from these radical-radical combination reactions and instead form via, e.g., the HACA mechanism. Species at 266 and 278 u, however, formed at significant amounts from radical-radical combination reactions, increasing the amount of mass 266 u by 35% and the amount of mass 278 u by over 1133% at 3.4 mm. The vast majority of the radicals that combined to form species of masses 266 and 278 u contained at least one pericondensed ring and about half of the radicals were PAH radicals. These computational results indicate that masses 266 u and 278 u could have comparable concentrations to some smaller masses, such as 202 u, at small HABs. In the case of 278 u, ~93% of the species skip traditional HACA pathways and form via radical-radical combination reactions that mainly involve at least one PAH radical in the size range from naphthyl to pyracyclene radicals. For species at 266 u, ~26% have undergone radical-radical combination reactions that often include at least one PAH radical in the size range from acenaphthylene radicals to the radicals of vinyl substituted cyclopenta[cd]pyrene. The importance of the PAH radical-radical reaction pathways depends on the distribution of radical species at a given point in the flame; frequent combinations will be effective at changing the mass frequency distribution. The concentration of PAH radicals is small compared to smaller reactive species, such as acetylene, which fuels the competing HACA mechanism, and the most relevant effects are observed when the small collision frequency is offset by a substantial increase in mass. For these reasons, the impact of "non-sequential" growth via PAH radical-radical combination is higher at higher HABs. This pathway to larger PAH production could be important in soot formation.

***Exploring the limitations of the stabilomer grid*:**[8b, 8c, 13] Many studies of incipient-particle composition employ AMS. For large hydrocarbon species, however, molecular structures cannot be identified by mass alone. Mass-resolved studies of soot constituents are often interpreted assuming that the major observed masses are stabilomers,[14] a class of species containing the most thermodynamically stable hydrocarbons.[15] Our work has shown that this assumption is not always valid. For example, the peak at 202 u (e.g., Fig. 7) is often assumed to be pyrene,[5b, 8a, 14b-d] and soot models frequently use pyrene as the nucleation seed species for soot inception.[2, 12, 16] By tuning the VUV photon energy, we measured the photoionization efficiency (PIE) as a function of photon energy of pure pyrene and of mass 202 u in our AMS spectra for several HABs. The results are shown in Fig. 9. The PIE curve shape is independent of HAB in this flame. The significant difference in the PIE curve shapes between pyrene and the flame shows that the 202-u peak in the flame contains a significant fraction of signal from pyrene isomers.

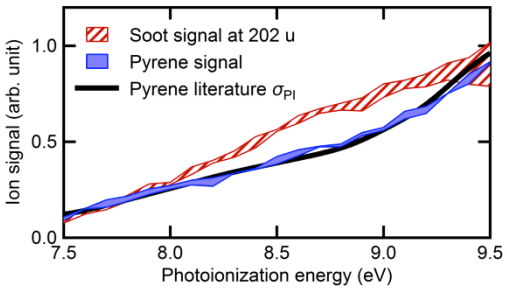

Figure 4.1.9. The hatched curve shows the lower and upper bounds of four PIE scans for the mass peak at 202 u recorded at HABs of 3.4, 5.4, and 9.4 mm in the premixed ethylene flame. The solid blue curve displays the bounds for two PIE scans performed on pyrene, and the black line is the normalized pyrene photoionization cross section (σ_{PI}) from Verstraete *et al.*[17] This figure is from Johansson *et al.*[8b]

To critically assess the potential of PIE analysis for isomer separation of hydrocarbon species with more than ~15 carbon atoms and to gain more information about the mass peak at 202 u, we calculated the ionization energies of 20 potential soot precursors with this mass and measured the absolute photoionization cross section of two likely candidates, pyrene and fluoranthene. Figure 10 shows a comparison of the PIE curves of these species with flame data at two HABs in the premixed ethylene flame.

A linear combination of these curves can reproduce the flame data. This analysis is consistent with the 202-u peak from the flame being composed of both species but does not definitively identify these species as the only isomers at this mass in the flame. The calculations of ionization energies of other potential isomers suggest that several other species may have similar PIE curves. In addition, the 20 isomers considered in the present analysis is only a small fraction of 202-u isomers.

Hence, these results illustrate the difficulty with establishing a definitive identification of isomers contributing to these large masses in flames. Nevertheless, they also demonstrate that PIE curves can be used to gain some information about these isomers, for example, by ruling out contributions from some isomers or combinations of isomers.

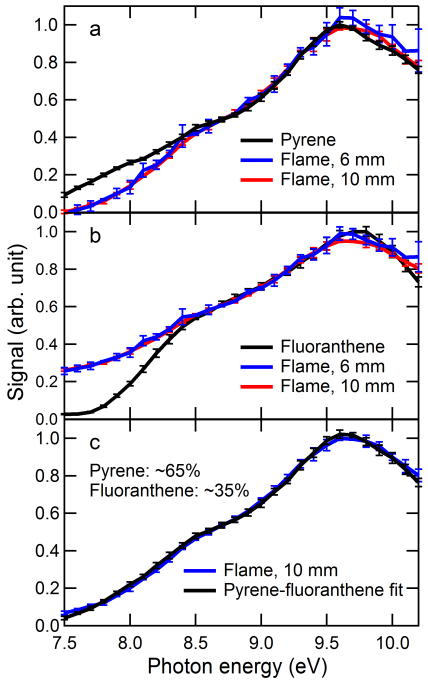

Figure 10. Comparison of flame PIE and known PAH-PIE curves for mass 202 u. Flame samples were extracted from the premixed ethylene flame at HABs of 6 and 10 mm. (a) Comparison between the shapes of the recorded pyrene-PIE curve and the flame-PIE curves of soot samples drawn from the flame. The flame-PIE curves were scaled and offset to agree with the pyrene-PIE curve between 8.5 and 9.5 eV. (b) Same as in (a), but with the flame-PIE curves normalized to the fluoranthene-PIE curve. (c) Comparison between the flame-PIE curve recorded from samples drawn at an HAB of 10 mm and the best fit of the PAH curves to the flame curve using a linear combination of the pyrene and fluoranthene-PIE curves. This figure is from Johansson *et al*.[13]

The interpretation of measurements in which particles are extracted from the flame is complicated by condensation in or on the probe that is inserted into the flame. In AMS instruments employing an aerodynamic lens system (ADL), efficient detection requires that the species either be in the particle in the flame or condense onto particles near the probe or inside the probe and sampling line and remain condensed all the way to the ionization region where it vaporizes. Molecules that do not condense and thus enter the ADL in the gas phase will not be focused by the ADL and are therefore unlikely to make it to the ionization region. A typical size-limit for ADL transmission efficiency is ~50 nm, below which particles are not likely to be detected.[18] Detection of smaller particles relies on coalescence, condensation, and/or coagulation in the sampling line. Thus, some species may be in the gas phase at flame temperatures but are nevertheless detected in the aerosol mass spectrometer. Laser-desorption mass spectrometry suffers from similar issues related to detection of species that are in the gas phase in the flame but condense onto the cooler target. Distinguishing between gas-phase and condensed-phase species in the flame is extremely difficult.

In order to test the hypothesis that the species with mass 202 u is in the gas phase in the flame, we installed a thermal denuder with the hottest section heated to a temperature of ~175 ˚C (close to atmospheric pressure) in front of the inlet nozzle to the aerosol mass spectrometer. A thermal denuder removes volatile particle coatings by vaporizing volatile species from particle surfaces. Vaporized hydrocarbon species are then trapped by activated carbon along the inner walls of the thermal denuder. Figure 11 shows mass spectra without and with the thermal denuder. Without the thermal denuder, the peak at 202 u is prominent, but it is negligibly small with the thermal denuder installed. This result demonstrates that, with moderate heating, the peak disappears, confirming that the species comprising this peak are in the gas-phase at high temperatures and condense in the cool probe.

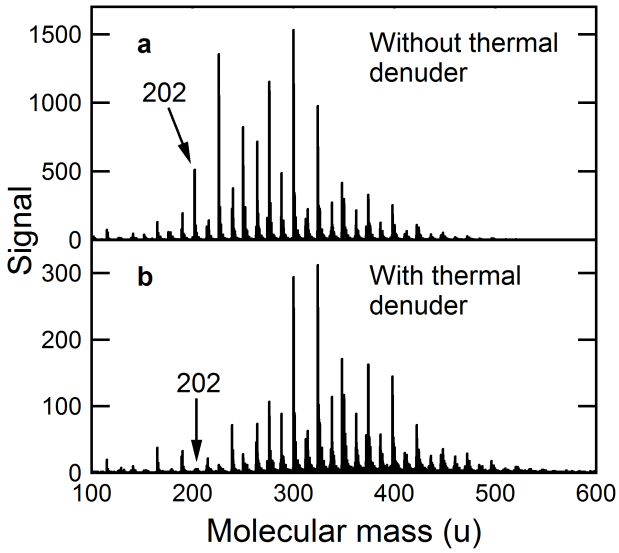

Figure 11. Aerosol mass spectra recorded in the premixed ethylene flame (a) without and (b) with a thermal denuder in front of the mass spectrometer. Mass spectra were recorded on particles extracted at an HAB of 6 mm. This figure is from Johansson *et al*.[13]

Thus, although pyrene is considered to be important for initiating soot nucleation in many models, the peak at mass 202 u is not entirely pyrene. Whether pyrene or not, it does not appear to condense at flame temperatures. The peak at mass 300 u similarly appears not to be consistent with the commonly assumed identity of coronene. Peaks with masses of 300 u and higher do not disappear in the thermal denuder and thus remain condensed on particles at higher temperatures than in the thermal denuder.

Literature Cited

1. (a) Frenklach, M.; Wang, H., Detailed modeling of soot particle nucleation and growth. *Twenty-Third Symp. (Int.) Combust.* **1991,** *23*, 1559-1566; (b) Richter, H.; Howard, J. B., Formation of polycyclic aromatic hydrocarbons and their growth to soot - a review of chemical reaction pathways. *Prog. Energy Combust. Sci.* **2000,** *26*, 565-608.

2. Frenklach, M., Reaction mechanism of soot formation in flames. *Phys. Chem. Chem. Phys.* **2002,** *4* (11), 2028-2037.

3. (a) Elvati, P.; Violi, A., Thermodynamics of poly-aromatic hydrocarbon clustering and the effects of substituted aliphatic chains. *Proc. Combust. Inst.* **2013,** *34* (1), 1837-1843; (b) Wang, H., Formation of nascent soot and other condensed-phase materials in flames. *Proc. Combust. Inst.* **2011,** *33*, 41-67; (c) Totton, T. S.; Misquitta, A. J.; Kraft, M., A quantitative study of the clustering of polycyclic aromatic hydrocarbons at high temperatures. *Phys. Chem. Chem. Phys.* **2012,** *14*, 4081-4094.
4. Weilmünster, P.; Keller, A.; Homann, K.-H., Large molecules, radicals, ions, and small soot particles in fuel-rich hydrocarbon flames Part I: Positive ions of polycyclic aromatic hydrocarbons (PAH) in low-pressure premixed flames of acetylene and oxygen. *Combust. Flame* **1999,** *116*, 62-83.
5. (a) Lowe, J. S.; Lai, J. Y. W.; Elvati, P.; Violi, A., Towards a predictive model for polycyclic aromatic hydrocarbon dimerization propensity. *Proc. Combust. Inst.* **2015,** *35*, 1827-1832; (b) Cain, J. P.; Laskin, A.; Kholghy, M. R.; Thomson, M. J.; Wang, H., Molecular characterization of organic content of soot along the centerline of a coflow diffusion flame. *Phys. Chem. Chem. Phys.* **2014,** *16*, 25862-25875.
6. (a) Skeen, S. A.; Michelsen, H. A.; Wilson, K. R.; Popolan, D. M.; Violi, A.; Hansen, N., Near-threshold photoionization mass spectra of combustion-generated high-molecular-weight soot precursors. *J. Aerosol Sci.* **2013,** *58*, 86-102; (b) D'Anna, A.; Violi, A., A kinetic model for the formation of aromatic hydrocarbons in premixed laminar flames. *Twenty-Seventh Symp. (Int.) Combust.* **1998,** *27* (1), 425-433; (c) Chung, S.-H.; Violi, A., Peri-condensed aromatics with aliphatic chains as key intermediates for the nucleation of aromatic hydrocarbons. *Proc. Combust. Inst.* **2011,** *33* (1), 693-700.
7. (a) D'Alessio, A.; D'Anna, A.; Gambi, G.; Minutolo, P., The spectroscopic characterisation of UV absorbing nanoparticles in fuel rich soot forming flames. *J. Aerosol Sci.* **1998,** *29* (4), 397-409; (b) Rusciano, G.; De Luca, A. C.; D'Alessio, A.; Minutolo, P.; Pesce, G.; Sasso, A., Surface-enhanced Raman scattering study of nano-sized organic carbon particles produced in combustion processes. *Carbon* **2008,** *46* (2), 335-341.
8. (a) Maricq, M. M., An examination of soot composition in premixed hydrocarbon flames via laser ablation particle mass spectrometry. *J. Aerosol Sci.* **2009,** *40*, 844-857; (b) Johansson, K. O.; Dillstrom, T.; Elvati, P.; Campbell, M. F.; Schrader, P. E.; Popolan-Vaida, D. M.; Hendersen-Richards, N. K.; Wilson, K. R.; Violi, A.; Michelsen, H. A., Radical-radical reactions, pyrene nucleation, and incipient soot formation in combustion. *Proc. Combust. Inst.* **2017,** *36*, in press; (c) Johansson, K. O.; Lai, J. Y. W.; Skeen, S. A.; Popolan-Vaida, D. M.; Wilson, K. R.; Hansen, N.; Violi, A.; Michelsen, H. A., Soot precursor formation and limitations of the stabilomer grid. *Proc. Combust. Inst.* **2015,** *35*, 1819-1826.
9. Johansson, K. O.; Dillstrom, T.; Monti, M.; El Gabaly, F.; Campbell, M. F.; Schrader, P. E.; Popolan-Vaida, D. M.; Richards-Henderson, N. K.; Wilson, K. R.; Violi, A.; Michelsen, H. A., Formation and emission of large furans and oxygenated hydrocarbons from flames. *P. Natl. Acad. Sci. USA* **2016,** *113* (30), 8374-8379.
10. (a) Peterson, L. A., Electrophilic Intermediates Produced by Bioactivation of Furan*. *Drug Metab. Rev.* **2006,** *38* (4), 615-626; (b) Ravindranath, V.; Burka, L. T.; Boyd, M. R., Reactive Metabolites from the Bioactivation of Toxic Methylfurans. *Science* **1984,** *224*, 884-886; (c) Monien, B. H.; Hermann, K.; Florian, S.; Glatt, H., Metabolic activation of furfuryl alcohol: formation of 2-methylfuranyl DNA adducts in Salmonella typhimurium strains expressing human sulfotransferase 1A1 and in FVB/N mice. *Carcinogenesis* **2011**, bgr126; (d) NIH *Toxicology and Carcinogenesis Studies of Furan (CAS No. 110-00-9) in F344 Rats and B6C3F1*

Mice (Gavage Studies); 0888-8051; 1993; pp 1-290; (e) WHO *IARC monographs on the evaluation of carcinogenic risks to humans, Internal report 14/002*; Lyon, France, 2014.
11. (a) Siegmann, K.; Hepp, H.; Sattler, K., Reactive dimerization: A new PAH growth mechanism in flames. *Combust. Sci. Technol.* **1995,** *109*, 165-181; (b) Sarofim, A. F.; Longwell, J. P.; Wornat, M. J.; Mukherjee, J., The role of biaryl reactions in PAH and soot formation. In *Soot Formation in Combustion*, Bockhorn, H., Ed. Springer-Verlag: Berlin, 1994; pp 485-499.
12. Schuetz, C. A.; Frenklach, M., Nucleation of soot: Molecular dynamics simulations of pyrene dimerization. *Proc. Combust. Inst.* **2002,** *29* (2), 2307-2314.
13. Johansson, K. O.; Campbell, M. F.; Elvati, P.; Schrader, P. E.; Jasper, A.; Zádor, J.; Richards-Henderson, N. K.; Wilson, K. R.; Violi, A.; Michelsen, H. A., Photoionization efficiencies of five polycyclic aromatic hydrocarbons and photoionization measurements on soot-precursor species. *J. Phys. Chem. A* **2017**, submitted.
14. (a) Faccinetto, A.; Desgroux, P.; Ziskind, M.; Therssen, E.; Focsa, C., High-sensitivity detection of polycyclic aromatic hydrocarbons adsorbed onto soot particles using laser desorption/laser ionization/time-of-flight mass spectrometry: An approach to studying the soot inception process in low-pressure flames. *Combust. Flame* **2011,** *158*, 227-239; (b) Dobbins, R. A.; Fletcher, R. A.; Chang, H.-C., The evolution of soot precursor particles in a diffusion flame. *Combust. Flame* **1998,** *115*, 285-298; (c) Maricq, M. M., Physical and chemical comparison of soot in hydrocarbon and biodiesel fuel diffusion flames: A study of model and commercial fuels. *Combust. Flame* **2011,** *158*, 105-116; (d) Bouvier, Y.; Mihesan, C.; Ziskind, M.; Therssen, E.; Focsa, C.; Pauwels, J. F.; Desgroux, P., Molecular species adsorbed on soot particles issued from low sooting methane and acetylene laminar flames: A laser-based experiment. *Proc. Combust. Inst.* **2007,** *31*, 841-849.
15. Stein, S. E.; Fahr, A., High-temperature stabilities of hydrocarbons. *J. Phys. Chem.* **1985,** *89*, 3714-3725.
16. (a) Mosbach, S.; Celnik, M. S.; Raj, A.; Kraft, M.; Zhang, H. R.; Kubo, S.; Kim, K.-O., Towards a detailed soot model for internal combustion engines. *Combust. Flame* **2009,** *156*, 1156-1165; (b) Sabbah, H.; Biennier, L.; Klippenstein, S. J.; Sims, I. R.; Rowe, B. R., Exploring the role of PAHs in the formation of soot: Pyrene dimerization. *J. Phys. Chem. Lett.* **2010,** *1* (19), 2962-2967.
17. Verstraete, L.; Leger, A.; d'Hendecourt, L.; Defourneau, D.; Dutuit, O., Ionization cross-section measurements for two PAH molecules-Implications for the heating of diffuse interstellar gas. *Astron. Astrophys.* **1990,** *237*, 436-444.
18. Liu, P. S. K.; Deng, R.; Smith, K. A.; Williams, L. R.; Jayne, J. T.; Canagaratna, M. R.; Moore, K.; Onasch, T. B.; Worsnop, D. R.; Deshler, T., Transmission efficiency of an aerodynamic focusing lens system: Comparison of model calculations and laboratory measurements for the Aerodyne Aerosol Mass Spectrometer. *Aerosol Science and Technology* **2007,** *41* (8), 721-733.

Publications from Support (2013 – 2016)

a) Johansson, K. O.; El Gabaly, F.; Schrader, P. E.; Campbell, M. F.; Michelsen, H. A., Evolution of particle surface and bulk maturity level during soot growth and oxidation in a flame. *Aerosol Sci. Technol.* **2017**, submitted. – Johansson supported by this project; El Gabaly, Schrader, Campbell, Michelsen was supported by other funding.

b) Johansson, K. O.; Campbell, M. F.; Elvati, P.; Schrader, P. E.; Zádor, J.; Richards-Henderson, N. K.; Wilson, K. R.; Violi, A.; Michelsen, H. A., Photoionization efficiencies of five polycyclic aromatic hydrocarbons. *J. Phys. Chem. A* **2017**, submitted. – Johansson, Elvati, Violi were supported by this project; Campbell, Schrader, Zádor, Michelsen, Wilson, Richards-Henderson were supported by other funding.

c) Johansson, K. O.; Zádor, J.; Elvati, P.; Campbell, M. F.; Schrader, P. E.; Richards-Henderson, N. K.; Wilson, K. R.; Violi, A.; Michelsen, H. A., Critical assessment of photoionization efficiency measurements for characterization of soot-precursor species. *J. Phys. Chem. A* **2017**, submitted. – Johansson, Elvati, Violi were supported by this project; Campbell, Schrader, Zádor, Michelsen, Wilson, Richards-Henderson were supported by other funding.

d) Campbell, M. F.; Bohlin, A.; Schrader, P. E.; Bambha, R. P.; Kliewer, C. J.; Johansson, K. O.; Michelsen, H. A., Design and characterization of a linear Hencken-type burner. *Rev. Sci. Instrum.* **2016**, *87*, 115114. – Johansson supported by this project; Campbell, Bohlin, Schrader, Kliewer, Michelsen, Bambha were supported by other funding.

e) Johansson, K. O.; Dillstrom, T.; Elvati, P.; Campbell, M. F.; Schrader, P. E.; Popolan-Vaida, D. M.; Richards-Henderson, N. K.; Wilson, K. R.; Violi, A.; Michelsen, H. A., Radical-radical reactions, pyrene nucleation, and incipient soot formation in combustion. *Proc. Combust. Inst.* **2016**, *36*, 799-806. Johansson, Dillstrom, Elvati, Violi were supported by this project; Campbell, Schrader, Michelsen, Wilson, Popolan-Vaida, Richards-Henderson were supported by other funding.

f) Johansson, K. O.; Dillstrom, T.; Campbell, M. F.; Monti, M.; El Gabaly, F.; Schrader, P. E.; Popolan-Vaida, D. M.; Richards-Henderson, N. K.; Wilson, K. R.; Violi, A.; Michelsen, H. A., Formation and emission of large furans and oxygenated hydrocarbons from flames *Proc. Natl. Acad. Sci. USA* **2016**, *113*, 8374-8379. Johansson, Dillstrom, Violi were supported by this project; Campbell, Monti, El Gabaly, Schrader, Michelsen, Wilson, Popolan-Vaida, Richards-Henderson were supported by other funding.

g) Johansson, K. O.; Lai, J. Y. W.; Skeen, S. A.; Popolan-Vaida, D. M.; Wilson, K. R.; Hansen, N.; Violi, A.; Michelsen, H. A., Soot precursor formation and limitations of the stabilomer grid. *Proc. Combust. Inst.* **2015**, *35*, 1819-1826. Johansson, Skeen, Lai, Violi were supported by this project; Michelsen, Wilson, Popolan-Vaida were supported by other funding.

h) Hansen, N.; Skeen, S. A.; Michelsen, H. A.; Wilson, K. R.; Kohse-Höinghaus, K., Flame experiments at the Advanced Light Source: New insights into soot formation processes. *J. Vis. Exp. (JoVE)* **2014**, *87*, e51369. Skeen was supported by this project; Hansen, Michelsen, Wilson, Kohse-Höinghaus were supported by other funding.

i) Skeen, S. A.; Michelsen, H. A.; Wilson, K. R.; Popolan, D. M.; Violi, A.; Hansen, N., Near-threshold photoionization mass spectra of combustion-generated high-molecular-weight soot precursors. *J. Aerosol Sci.* **2013**, *58*, 86-102. Skeen, Violi were supported by this project; Hansen, Michelsen, Wilson, Popolan were supported by other funding.

j) Skeen, S. A.; Yang, B.; Michelsen, H. A.; Miller, J. A.; Violi, A.; Hansen, N., Studies of laminar opposed-flow diffusion flames of acetylene at low pressures with photoionization mass spectrometry. *Proc. Combust. Inst.* **2013**, *34*, 1067-1075. Skeen, Violi was supported by this project; Hansen, Michelsen, Miller, Yang were supported by other funding.